Calibration of strapdown magnetic vector measurement systems based on a plane compression method

To cite this article: Supeng Li *et al* 2023 *Meas. Sci. Technol.* **34** 055115

View the article online for updates and enhancements.

Calibration of strapdown magnetic vector measurement systems based on a plane compression method

Supeng Li[1] , **Defu Cheng**[1,2]**, Yi Wang**[1] **and Jing Zhao**[1,2,*]

[1] College of Instrumentation and Electrical Engineering, Jilin University, Changchun, People's Republic of China
[2] Key Laboratory of Geophysical Exploration Equipment, Jilin University, Changchun, People's Republic of China

E-mail: zhaojing_8239@jlu.edu.cn

CrossMark

Abstract

The strapdown magnetic vector measurement system, which can measure the magnetic vector and the attitude of a magnetometer simultaneously, has wide applications in geophysical prospecting, etc. Calibration of systematic errors, including magnetometer errors and misalignment errors, is essential for this system. Traditional methods calibrate these two errors separately, with the problem of cumbersome steps and being dependent on special data acquisition methods, such as rotation. An original method that combines a plane compression method with an ellipsoid fitting method is proposed in this paper, which can simultaneously complete the calibration calculation of magnetometer error and misalignment error in one experiment. The calculation can be performed using the spatial scatter point data required by the traditional attitude-independent magnetometer calibration method, and no additional mechanical equipment is required. A mathematical analysis of this method is performed to study the elements decreasing the measurement accuracy of the system, and numerical simulation and field experiments are performed to validate the analysis. The results indicate that the method can contribute to the accuracy improvement of magnetic vector measurement systems.

Keywords: magnetic vector measurement system, magnetometer error, misalignment error, inertial navigation system

(Some figures may appear in colour only in the online journal)

1. Introduction

The strapdown magnetic vector measurement system composed of a triaxial magnetometer and inertial navigation system (INS) can measure the east, north and vertical components of a magnetic vector, which makes it more attractive than scalar magnetic measurement in geomagnetic navigation [1–3], magnetic anomaly detection [4, 5] and underground mineral exploration [6, 7].

The magnetometer obtains the three-axis projections of the local magnetic field under its own coordinate, and then it is restored to the geographic coordinate according to the attitude information provided by the INS. However, the errors in the system will affect the measurement accuracy. First, the triaxial magnetometer has inherent errors, including the offset error, scale factor error and orthogonality error. Second, there is a misalignment error between the magnetometer and the INS. Since the above errors can cause thousands of nT deviations, calibration

* Author to whom any correspondence should be addressed.

is essential before using the magnetic vector measurement system.

In previous research, the calibration of the triaxial magnetometer has been proposed and researched in depth [8–15]. The earliest solutions were to use a known magnetic source for magnetometer calibration [8, 9]. However, these methods need to be conducted in a shielded chamber environment and have a high requirement for the precision of magnetic source generating equipment. The next generation methods are attitude-independent calibration using the geomagnetic field *in situ*, which was first proposed by Merayo in 2000 [10]. The recent attitude-independent magnetometer calibration methods are mainly ellipsoid fitting methods based on least squares [11–15]. These two kinds of methods can achieve great calibration accuracy, but they cannot solve the misalignment error in the magnetic vector measurement system. As a result, the components of the calibrated magnetic data will still have large fluctuations after they are restored to the geographic coordinate.

Due to the need for installation, the three axes of the magnetometer and the three axes of the INS are not completely aligned, which results in the misalignment error. The sensitive axes of the above sensors are both inside and have no connection with the orientation of their shell body. Therefore, the misalignment error is inevitable and cannot be eliminated by mechanical means. Since the post-processing of the three-component magnetic survey data needs to be restored to the geographic coordinate, it is particularly important that the attitude data can accurately reflect the orientation of the magnetometer. A series of methods were proposed by Li for calibration of the misalignment between the accelerometer coordinate and the magnetometer coordinate using the property whereby the dot product of the geomagnetic field and gravity field is constant [16, 17]. Pang proposed a hexahedron-device-assisted method to calibrate the misalignment error, but the method depends on the precision of the hexahedron auxiliary device [18]. Wan reported a method using the Lagrange multiplier to calculate the combined matrix of the magnetometer error and misalignment error. This method needs to rotate the system via a planar positioning device several times; thus, the calibration accuracy will be affected by the rotation plane [19]. Gao proposed a method to calibrate the misalignment error by constructing data plane normal vectors [20]. The problem with this method is that when the accuracy of the turntable is insufficient, the calibration accuracy will decrease. Together, these methods have achieved satisfactory results in calibration misalignment errors. However, the special data acquisition mode they have adopted can lead to a decrease in the accuracy of the calibration using the acquired data.

Compared with previous methods, the main aim of this paper is to propose a method that can simultaneously calibrate the magnetometer and misalignment error without the need for rotation or additional mechanical devices. Also, this method has potential application value for other sensor systems that need to use attitude data for coordinate projection. The paper is organized as follows. Section 2 analyses and models the errors of the magnetometer and misalignment. Section 3 illustrates the construction method of the calibration objective function proposed in this paper. Section 4 uses the simulation experiment to prove the theoretical feasibility of the method. Section 5 verifies the accuracy and robustness of the method in practical applications via a field experiment. Section 6 discusses the problems and potential of the proposed method. The conclusion is given in section 7.

2. Error modeling

Within a certain time, the geomagnetic field at the experimental site can be considered as a constant. The value is set as:

$$H_g = \begin{bmatrix} H_{gx} & H_{gy} & H_{gz} \end{bmatrix}^T \tag{1}$$

where H_{gx}, H_{gy}, H_{gz} denote the projection of the geomagnetic field in east, north and vertical directions of the geographic coordinate.

The projection of the geomagnetic field on the magnetometer coordinate can be obtained by Euler's rotation theorem [21]:

$$\begin{cases} H_g(i) = R(i) \cdot H_g \\ R(i) = R_y(\gamma_i) \cdot R_x(\beta_i) \cdot R_z(\alpha_i) \end{cases} \tag{2}$$

where α, β, γ denote the heading, pitch and roll angles provided by the INS, respectively. Here, i denotes the data points.

The misalignment error reflects the angular deviation between the magnetometer coordinate and the INS coordinate, which is constant after the installation of the magnetic vector measurement system. The definition of the three misalignment error angles is shown in figure 1.

Equation (2) can be improved to equation (3) by adding the misalignment error,

$$\begin{cases} H_{gm}(i) = R_m \cdot R(i) \cdot H_g \\ R_m = R_y(\gamma_m) \cdot R_x(\beta_m) \cdot R_z(\alpha_m) \end{cases} \tag{3}$$

where $\alpha_m, \beta_m, \gamma_m$ denote misalignment error angles.

Equation (3) can represent the theoretical value of the geomagnetic vector in the magnetometer coordinate, but the error of the magnetometer, which includes the scale factor error, orthogonal error and offset error, will lead to the deviation between the measured value and $H_{gm}(i)$.

The scaling factor error is the deviation of the scaling factor of the respective axis from the standard value, and its matrix form is shown in equation (4):

$$K_s = \text{diag}(\begin{array}{ccc} K_{sx} & K_{sy} & K_{sz} \end{array}). \tag{4}$$

The orthogonal error represents the angular deviation between the magnetometer coordinate and the orthogonal coordinate, and its schematic diagram is shown in figure 2.

We assume that the *x*-axis of the magnetometer coincides with an orthogonal coordinate. Here, O_1, O_2 and O_3 can represent the three angles that define the orthogonal error.
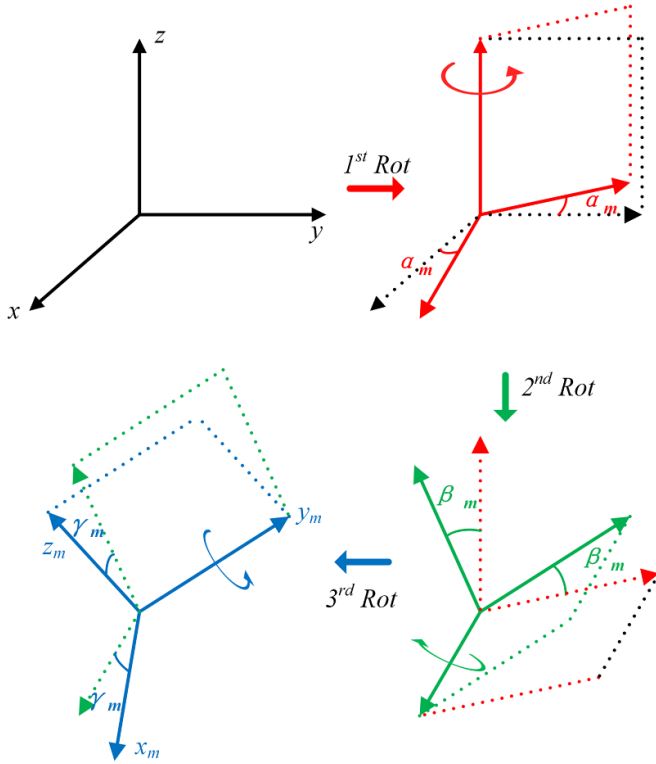
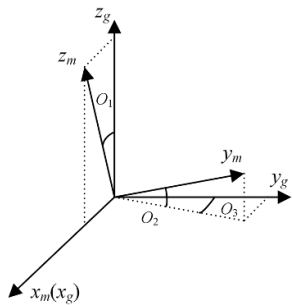**Figure 1.** The definition of misalignment error angles.

Figure 2. A diagram of the orthogonal error in the magnetometer.

Accordingly, the projection of the orthogonal coordinate system on the magnetometer coordinate can be expressed by equation (5):

$$K_o = \begin{bmatrix} 1 & 0 & 0 \\ \cos O_2 \sin O_3 & \cos O_2 \cos O_3 & \sin O_2 \\ \sin O_1 & 0 & \cos O_1 \end{bmatrix} \quad (5)$$

where K_o denotes the orthogonal error matrix.

The offset error can be regarded as:

$$K_{of} = \begin{bmatrix} K_{ofx} & K_{ofy} & K_{ofz} \end{bmatrix}^T \quad (6)$$

where K_{ofx}, K_{ofy}, K_{ofz} denote the offset error on the three axes of the magnetometer.

Based on the above analysis, the measured value of the magnetic vector measurement system, including magnetometer error and misalignment error, can be modeled as:

$$H_d(i) = K_s \cdot K_o \cdot R_m \cdot R(i) \cdot H_g + K_{of} \quad (7)$$

where H_d denotes the measured value of the magnetic vector measurement system.

3. Calibration method

Due to the fact that the exact geomagnetic vector H_g is unknown, equation (7) cannot be solved directly. Additional constraints are required to calculate the error parameters.

The deformation of equation (7) is as follows:

$$R(i)^{-1} \cdot R_m^{-1} \cdot K_o^{-1} \cdot K_s^{-1} \cdot (H_d(i) - K_{of}) = H_g. \quad (8)$$

Since the Euler rotation matrix is an orthogonal matrix, the dot product of its transposition with itself is the identity matrix. Accordingly, equation (9) can be obtained from equation (8),

$$\begin{aligned} \left[(H_d(i) - K_{of})^T \cdot G \cdot (H_d(i) - K_{of})/|H_g|^2 \right] - 1 = 0 \\ G = (K_s^{-1})^T \cdot (K_o^{-1})^T \cdot K_o^{-1} \cdot K_s^{-1} \end{aligned} \quad (9)$$

where

$$G = \begin{bmatrix} g_1 & g_4 & g_5 \\ g_4 & g_2 & g_6 \\ g_5 & g_6 & g_3 \end{bmatrix}.$$

Equation (9) is consistent with the equation of spatial ellipsoids, and G and K_{of} can be obtained using an ellipsoid fitting algorithm when $|H_g|$ is known [22]. The value of $|H_g|$ can be obtained by the magnetic total field magnetometer. Therefore, the objective function of the ellipsoid fitting method can be set as follows:

$$\varepsilon_1 = \min \left\{ \left[(H_d(i) - K_{of})^T \cdot G \cdot (H_d(i) - K_{of})/|H_g|^2 \right] - 1 \right\}. \quad (10)$$

The inverse matrix of K_s and K_o is set in equation (11):

$$K_o^{-1} = \begin{bmatrix} 1 & 0 & 0 \\ K_1 & K_2 & K_3 \\ K_4 & 0 & K_5 \end{bmatrix}$$

$$K_s^{-1} = \mathrm{diag}\begin{pmatrix} K_6 & K_7 & K_8 \end{pmatrix} \quad (11)$$

where

$$\begin{cases} K_1 = -\frac{\sin O_3}{\cos O_3} + \frac{\sin O_1 \sin O_3}{\cos O_1 \cos O_2 \cos O_3} & K_5 = \frac{1}{\cos O_1} \\ K_2 = \frac{1}{\cos O_2 \cos O_3} & K_6 = K_{sx}^{-1} \\ K_3 = -\frac{\sin O_2}{\cos O_1 \cos O_2 \cos O_3} & K_7 = K_{sy}^{-1} \\ K_4 = -\frac{\sin O_1}{\cos O_1} & K_8 = K_{sz}^{-1} \end{cases}.$$
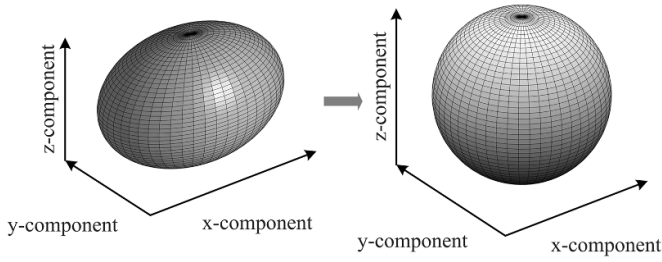
Figure 3. The data fitting diagram.

Figure 4. A schematic diagram of the misalignment error effect.

Matrix G can be expanded as:

$$G = \begin{bmatrix} K_1{}^2 K_7{}^2 + K_4{}^2 K_8{}^2 + K_6{}^2 & K_1 K_2 K_7{}^2 & K_1 K_3 K_7{}^2 + K_4 K_5 K_8{}^2 \\ K_1 K_2 K_7{}^2 & K_2{}^2 K_7{}^2 & K_2 K_3 K_7{}^2 \\ K_1 K_3 K_7{}^2 + K_4 K_5 K_8{}^2 & K_2 K_3 K_7{}^2 & K_3{}^2 K_7{}^2 + K_5{}^2 K_8{}^2 \end{bmatrix}.$$
(12)

The expressions for each element in the G matrix that can be obtained by equations (9) and (12) are as follows:

$$K_2 K_7 = \sqrt{g_2} \quad K_1 K_7 = \frac{g_4}{\sqrt{g_2}} \quad K_3 K_7 = \frac{g_6}{\sqrt{g_2}}$$

$$K_5 K_8 = \sqrt{g_3 - \frac{g_6{}^2}{g_2}} \quad K_4 K_8 = \frac{(g_2 g_5 - g_4 g_6)}{\sqrt{g_2{}^2 g_3 - g_2 g_6{}^2}} \quad .$$
(13)

$$K_6 = \sqrt{g_1 - \frac{g_4{}^2}{g_2} - \frac{(g_2 g_5 - g_4 g_6)^2}{g_2{}^2 g_3 - g_2 g_6{}^2}}$$

Substituting equation (11) into (13) gives the equation for the calculation of orthogonal error angles:

$$\begin{cases} O_1 = \arcsin\left(\frac{-K_4 K_8}{K_5 K_8}\right) \\ O_2 = \arcsin\left(\frac{-K_3 K_7 \cos O_1}{K_2 K_7}\right) \\ O_3 = \arccos\left(\frac{-K_5 K_7 \sin O_2}{K_3 K_7 \cos O_2}\right) \end{cases} .$$
(14)

When the O_1, O_2 and O_3 angles are known, K_{sx}, K_{sy} and K_{sz} can be solved by equations (11)–(13). So far, the error matrices K_o, K_s and K_{of} have been solved.

Set:

$$H_d'(i) = K_o{}^{-1} \cdot K_s{}^{-1} \cdot (H_d(i) - K_{of}).$$
(15)

The known magnetometer error matrices are brought into equation (15) to calculate the value of $H_d'(i)$.

Equation (16) can be obtained by deforming equation (7):

$$\begin{aligned} H_d'(i) &= R_m \cdot R(i) \cdot H_g \\ &= R_m \cdot R_y(\gamma_i) \cdot R_x(\beta_i) \cdot R_z(\alpha_i) \cdot H_g. \end{aligned}$$
(16)

After calibration using the ellipsoid fitting method, the trajectory formed by $H_d'(i)$ is a spatial sphere. The trajectory fitting graph of the data is shown in figure 3.

The sphere is formed by the projection of the geomagnetic field on the three axes of the magnetometer at different attitudes. Theoretically, we can restore the 3D sphere to a spatial
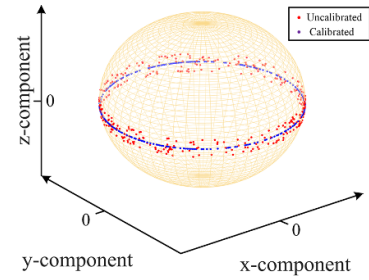
circle using Euler's rotation theorem. Its matrix form is shown as equation (17),

$$H_d''(i) = R_z(\alpha_i) \cdot H_g = R_x(\beta_i)^{-1} \cdot R_y(\gamma_i)^{-1} \cdot R_m{}^{-1} \cdot H_d'(i)$$
(17)

where i denotes the different magnetic data.

The unknown R_m matrix will cause the restoration result to deviate from the space circle, as shown in figure 4.

According to the rotation theorem, the trajectory formed by the rotation of a vector around a spatial axis is a spatial circle perpendicular to the rotation axis. The lines on the spatial circle can be obtained by vector subtraction. Equation (18), constructed by the normal vector theorem, is as follows:

$$f(i,j) = \begin{bmatrix} 0 & 0 & 1 \end{bmatrix} \cdot (H_d''(i) - H_d''(j)).$$
(18)

To simplify the expression, we set:

$$\begin{bmatrix} 0 & 0 & 1 \end{bmatrix} \cdot R_x(\beta_i) \cdot R_y(\gamma_i) = \begin{bmatrix} a_i & b_i & c_i \end{bmatrix} = Q(i).$$
(19)

Substituting equation (19) into equation (18) for matrix calculation leads to equation (20):

$$f(i,j) = \left(Q(i) \cdot R_m{}^{-1} \cdot H_d'(i) - Q(j) \cdot R_m{}^{-1} \cdot H_d'(j)\right)$$
(20)

where i and j denote the data points.

The value of $f(i, j)$ is zero when all points lie on the spatial circle. Then, the calibration of the misalignment error angles is transformed into a ternary nonlinear equation after this derivation. Theoretically, it can be solved using a simple nonlinear least square method with the measured data of three different attitudes. However, calculations with too little data will cause the random errors of the INS to seriously interfere with the results. To enhance the anti-interference ability of the calibration algorithm, 30 points data are used in one experiment. Based on the principle of pairwise subtraction of vectors, $C_{30}^2 = 435$ equations can be constructed. The objective function to solve this problem is set as follows:

$$\varepsilon_2 = \min\left(\sum_{i=1}^{n} \sum_{j=i+1}^{n} f(i,j)\right).$$
(21)

After the above analysis, the final objective function $\varepsilon = \varepsilon_{1*}\varepsilon_2$ is used to calculate the calibration parameters.

4. Simulation

In this section, numerical simulation experiments are carried out to verify the theoretical feasibility of the proposed method.

4.1. Simulation setting

In the simulation, we set up two different sets of background geomagnetic vector fields to verify the effectiveness of the proposed method when the background geomagnetic vector field at the experimental site changes due to magnetic anomalies. According to the actual local magnetic field, the first set of the geomagnetic vector field is assumed to be $H_{g1} = [25\,022\ {-4053}\ 47\,374]$ and the $|H_{g1}|$ value is calculated as 53 729.2 nT. Magnetic anomalies were added to the first set of data to generate the second set of data. We assume that the magnetic vector of the magnetic anomaly at the experimental site is $[-917\ 530\ {-5251}]$. The second set of geomagnetic fields can be calculated as $H_{g2} = [24\,105\ {-3523}\ 42\,123]$ and the $|H_{g2}|$ value is 48 020.4 nT. These two sets of background geomagnetic vector fields will generate simulation data using the same error parameters.

Misalignment error angles and orthogonal error angles are set as:

$$\begin{bmatrix} O_1 & O_2 & O_3 \end{bmatrix} = \begin{bmatrix} 1.7° & 3.5° & 2.1° \end{bmatrix}$$
$$\begin{bmatrix} \alpha_m & \beta_m & \gamma_m \end{bmatrix} = \begin{bmatrix} 5.7° & 2.1° & 3.5° \end{bmatrix}.$$

Therefore, the misalignment error and orthogonal error matrices are obtained according to the preset values:

$$R_m = \begin{bmatrix} 0.9934 & -0.0969 & 0.0610 \\ 0.0993 & 0.9944 & -0.0367 \\ -0.0571 & 0.0425 & 0.9975 \end{bmatrix}$$

$$K_o = \begin{bmatrix} 1 & 0 & 0 \\ 0.0365 & 0.9975 & 0.0366 \\ 0.0297 & 0 & 0.9996 \end{bmatrix}.$$

The scaling factor error and bias error are set to:

$$K_s = \begin{bmatrix} 1.08 & 0 & 0 \\ 0 & 1.02 & 0 \\ 0 & 0 & 1.033 \end{bmatrix} \quad K_{of} = \begin{bmatrix} 4.9 \\ 3.4 \\ 0.7 \end{bmatrix}.$$

The noise of the magnetometer was set as white Gaussian noise with zero mean and its standard deviation (SD) was 0.3 nT. The error of the attitude angles from the INS was set as the mean value of 0 and the SD value of 0.015°. Sixty groups of attitude angles are generated randomly. The simulation data can be obtained by substituting these preset values into equation (7).

4.2. Simulation results

The simulation data use the MATLAB program for calibration calculation. The calibration results are shown below:

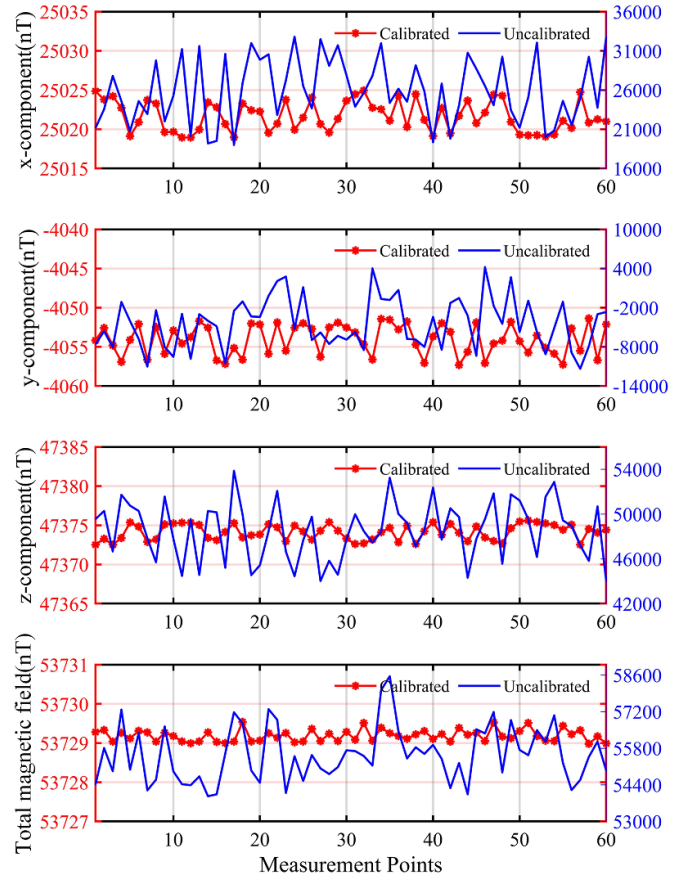Dataset 1: A comparison of the data before and after calibration is shown in figure 5.

Figure 5. Calibration results of dataset 1.

The error parameters obtained by solving the first set of simulation data using the proposed method are:

$$\begin{bmatrix} \alpha_m & \beta_m & \gamma_m \end{bmatrix} = \begin{bmatrix} 5.7002° & 2.1006° & 3.4947° \end{bmatrix}$$

$$R_m = \begin{bmatrix} 0.9934 & -0.0969 & 0.0609 \\ 0.0993 & 0.9944 & -0.0367 \\ -0.0570 & 0.0425 & 0.9975 \end{bmatrix}$$

$$\begin{bmatrix} O_1 & O_2 & O_3 \end{bmatrix} = \begin{bmatrix} 1.6998° & 3.5134° & 2.1006° \end{bmatrix}$$

$$K_o = \begin{bmatrix} 1.0000 & 0 & 0 \\ 0.0366 & 0.9976 & 0.0367 \\ 0.0297 & 0 & 0.9996 \end{bmatrix}$$

$$K_{sf} = \begin{bmatrix} 1.0800 & 0 & 0 \\ 0 & 1.0199 & 0 \\ 0 & 0 & 1.0330 \end{bmatrix} \quad K_{of} = \begin{bmatrix} 4.8171 \\ 3.4128 \\ 0.7585 \end{bmatrix}.$$

Dataset 2: A comparison of the data before and after calibration is shown in figure 6.

The error parameters obtained by solving the second set of simulation data using the proposed method are:

$$\begin{bmatrix} \alpha_m & \beta_m & \gamma_m \end{bmatrix} = \begin{bmatrix} 5.6999° & 2.1007° & 3.4967° \end{bmatrix}$$

$$R_m = \begin{bmatrix} 0.9934 & -0.0969 & 0.0610 \\ 0.0992 & 0.9944 & -0.0367 \\ -0.0571 & 0.0425 & 0.9975 \end{bmatrix}$$
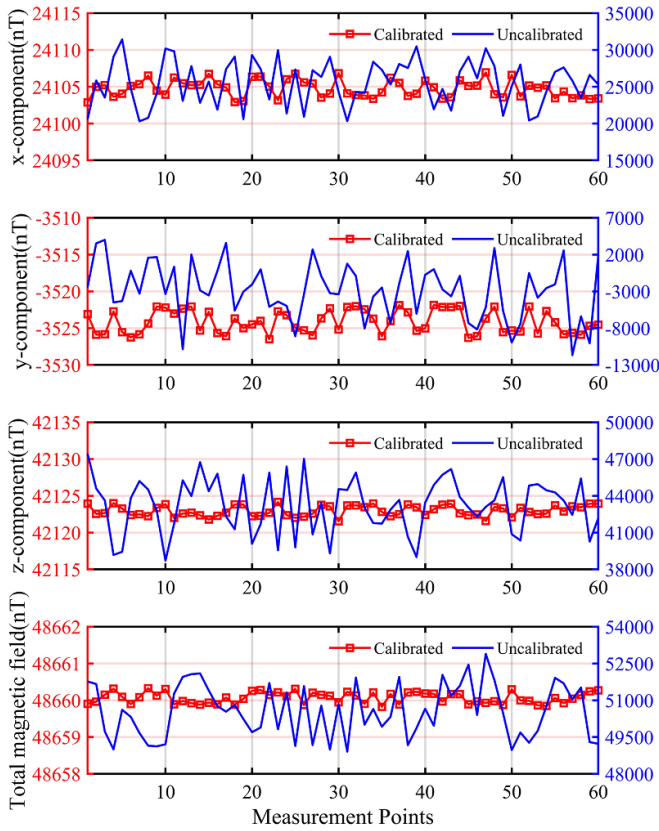
Figure 6. Calibration results of dataset 2.

$$
\begin{bmatrix} O_1 & O_2 & O_3 \end{bmatrix} = \begin{bmatrix} 1.6998° & 3.5132° & 2.1000° \end{bmatrix}
$$

$$
K_o = \begin{bmatrix} 1.0000 & 0 & 0 \\ 0.0366 & 0.9976 & 0.0366 \\ 0.0297 & 0 & 0.9996 \end{bmatrix}
$$

$$
K_{sf} = \begin{bmatrix} 1.0800 & 0 & 0 \\ 0 & 1.0199 & 0 \\ 0 & 0 & 1.0330 \end{bmatrix} \quad K_{of} = \begin{bmatrix} 4.8051 \\ 3.4112 \\ 0.7575 \end{bmatrix}.
$$

Comparing the estimated error parameters of both datasets with the preset values, the relative errors are less than 1.6% and 1.7%. The calibration parameters for these two data sets are almost identical, and the small deviations between them are mainly due to the random noise.

The difference between the data calibration effects of the two datasets was less than 0.1%. After calibration, the root mean square error (RMSE) of the three components and magnetic intensity are within 2 nT and 0.18 nT, respectively. The results show that the method can accurately calibrate the magnetic vector measurement system in any stable background magnetic field, and the calibrated magnetic vector data will always be concentrated around the true value after attitude recovery.

5. Field experiment

The field experiment data are used to verify the accuracy and reliability of the method in practical applications.
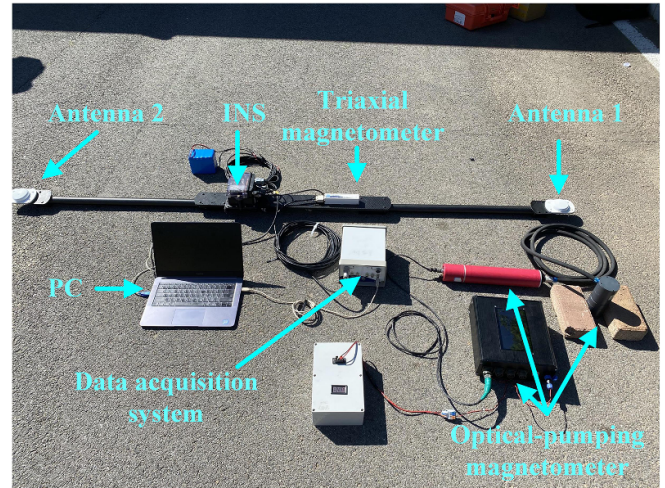

Figure 7. The experimental apparatus.

5.1. Experimental apparatus

The experimental apparatus included a triaxial magnetometer (Bartington), an INS (NovAtel), a carbon fiber board (to fix the magnetometer and INS), a Cs-3 optical-pumping magnetometer (to provide the geomagnetic total field value for calibration), a data acquisition system (to measure data) and data acquisition software. The experimental apparatus is shown in figure 7.

The performance specifications of the Mag-03 are: the measurement range is ±100 000 nT (component value); orthogonality is <0.1°; the scaling error is <0.5%; the offset error is <±5 nT; and the accuracy is ±1 nT. The performance specifications of the CS-3 optical-pumping magnetometer are: the measurement range is 15 000–105 000 nT, and the noise envelope is 0.002 nT peak-to-peak (0.1 Hz). The accuracy of the angle measurement of the INS is <0.015° (RMSE).

The field experiment was conducted in the suburb of Changchun with a stable magnetic environment. Before the experiment, we used a cs-3 optical-pumping magnetometer to explore the magnetic environment in the area. The local diurnal variation is less than 5 nT h⁻¹, the magnetic gradient is less than 68pT m⁻¹ and the geomagnetic intensity is 53 766.54 nT. Four replicate experiments were conducted at the experimental site to verify the robustness and accuracy of the proposed method. Each experiment collects 30 data for calibration calculation, and these data are evenly distributed in space.

5.2. Experimental results

After calculation using the method in this paper, the calibration parameters of all the experiments are shown in table 1.

Since it is nearly impossible to obtain the standard values of the magnetic vector field in the geographic coordinate, we cannot calculate the RMSE without the true value of the geomagnetic vector. In previous studies, researchers have tended to use the International geomagnetic reference field

Table 1. Calibration parameters.

S/N	1	2	3	4
K_{sf}	$\mathrm{diag}\begin{pmatrix} 1.0038 \\ 1.0011 \\ 1.0032 \end{pmatrix}$	$\mathrm{diag}\begin{pmatrix} 1.0038 \\ 1.0011 \\ 1.0031 \end{pmatrix}$	$\mathrm{diag}\begin{pmatrix} 1.0037 \\ 1.0013 \\ 1.0031 \end{pmatrix}$	$\mathrm{diag}\begin{pmatrix} 1.0038 \\ 1.0012 \\ 1.0031 \end{pmatrix}$
O	$\begin{bmatrix} 0.0282° \\ -0.0253° \\ 0.0470° \end{bmatrix}$	$\begin{bmatrix} 0.0287° \\ -0.0251° \\ 0.0470° \end{bmatrix}$	$\begin{bmatrix} 0.0288° \\ -0.0251° \\ 0.0473° \end{bmatrix}$	$\begin{bmatrix} 0.0274° \\ -0.0249° \\ 0.0451° \end{bmatrix}$
R_m	$\begin{bmatrix} 2.5902° \\ -1.7526° \\ -0.0437° \end{bmatrix}$	$\begin{bmatrix} 2.5920° \\ -1.7516° \\ -0.0447° \end{bmatrix}$	$\begin{bmatrix} 2.5875° \\ -1.7521° \\ -0.0432° \end{bmatrix}$	$\begin{bmatrix} 2.5838° \\ -1.7515° \\ -0.0426° \end{bmatrix}$
K_{of}	$\begin{bmatrix} 4.9830 \\ 1.2198 \\ 4.5971 \end{bmatrix}$	$\begin{bmatrix} 4.9831 \\ 1.2193 \\ 4.5980 \end{bmatrix}$	$\begin{bmatrix} 4.9803 \\ 1.2201 \\ 4.5451 \end{bmatrix}$	$\begin{bmatrix} 4.9861 \\ 1.2410 \\ 4.6558 \end{bmatrix}$

Table 2. The evaluation index of the three components.

Experiment number	No. 1			No. 2		
Components	x (nT)	y (nT)	z (nT)	x (nT)	y (nT)	z (nT)
Calibrated	4.6	2.5	1.6	5.7	2.8	1.7
Before calibration	1471.0	1000.1	785.7	1260.4	1236.3	680.2
Feature	Magnetic intensity (RMSE)			Magnetic intensity (RMSE)		
Calibrated	1.15			1.19		
Before calibration	51.29			51.80		
Experiment number	No. 3			No. 4		
Components	x (nT)	y (nT)	z (nT)	x (nT)	y (nT)	z (nT)
Calibrated	5.2	2.4	1.8	6.4	2.9	1.7
Before calibration	1461.2	870.9	807.4	1680.9	897.6	846.2
Feature	Magnetic intensity (RMSE)			Magnetic intensity (RMSE)		
Calibrated	1.08			1.55		
Before calibration	51.17			50.1		

(IGRF) model as the true value of magnetic vectors. However, the IGRF model deviates from the actual local magnetic field value. According to the data of 29 geomagnetic stations in China, the average RMSE of the IGRF model and measured values is 146.9 nT [23]. It is unfair to use it as an evaluation criterion for calibration effects. The fluctuations in the three-component magnetic field after recovery to the geographic coordinate system are caused by misalignment errors. The better the misalignment error calibration effect, the smaller the three-component fluctuation. This means that the dispersion of the calibrated data can reflect the calibration effect of the misalignment error. Therefore, the components' accuracy of the calibrated magnetic vector measurement system is evaluated using the SD value, and the RMSE is introduced to evaluate the calibration precision of the synthetic total magnetic field of the measurement data. The magnetic intensity measured by the CS-3 optical-pumping magnetometer was used as the magnetic field reference at the experimental site. The calibration results are shown in table 2.

In all four experiments, the average SD values of the three components of *x, y* and *z* decreased by 99.6%, 99.7% and

99.7%, respectively. The slight deviation of the results is attributed to the uncertain error of the INS. The RMSEs of the magnetic intensity after calibration for the four groups of experiments are 1.15 nT, 1.19 nT, 1.08 nT and 1.55 nT, respectively. The largest residual occurred in experiment No.4, which was caused by the insufficient coverage of the space by this set of data.

A comparative experiment was carried out to demonstrate the advantages of this method over traditional methods. The same data were calculated using the traditional attitude-independent calibration method as a comparison experiment. There are two main reasons for this choice. First, the previous misalignment error calibration methods cannot be calculated using the experimental data. Second, the magnetic vector measurement system cannot work in the shielded room environment without a global positioning system (GPS) signal, which makes it impossible to use the magnetic field generator to calibrate the system.

To visually demonstrate the calibration effect of the proposed method, the calibration results of experimental data No.4 using the proposed method and comparison method are shown in figure 8.
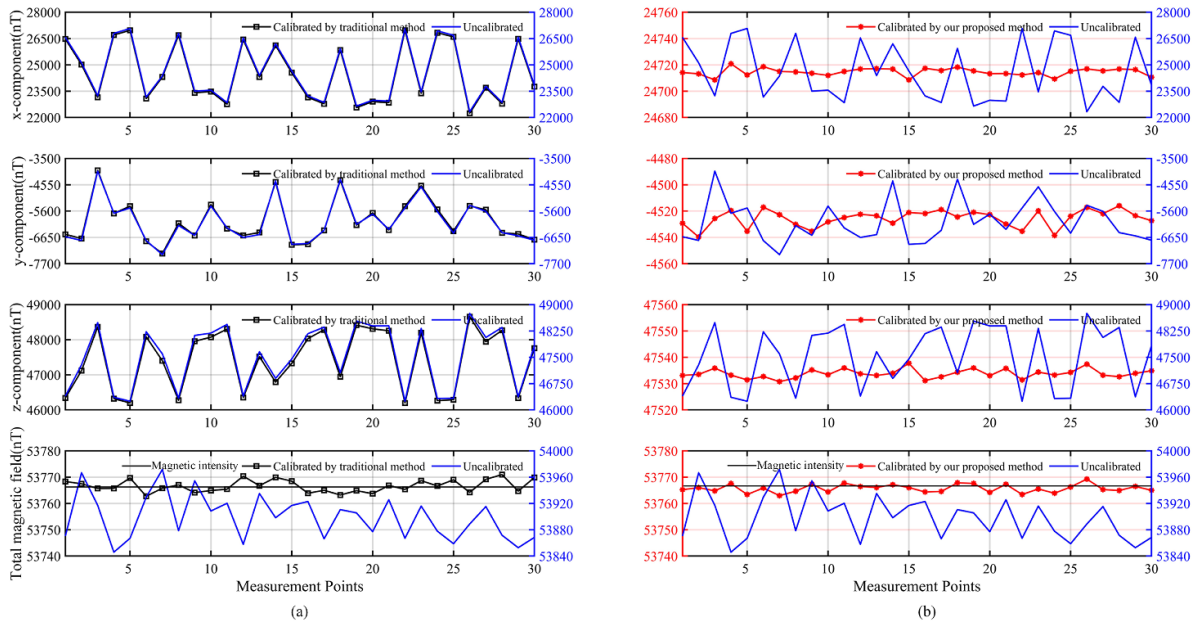
Figure 8. The calibration results of experimental data No.4. (a) The calibration results of the traditional ellipsoid fitting method. (b) The calibration results of the proposed method.

Table 3. Comparison of accuracy with different methods.

Feature	x (SD)	y (SD)	z (SD)	Magnetic intensity (RMSE)
Traditional ellipsoid fitting method	1675.6	871.2	842.6	1.58
Proposed method	6.4	2.9	1.7	1.55

The calibration results of the comparison method versus the experimental data are shown in table 3.

The results in figure 8 and table 3 show that the traditional attitude-independent calibration method is only valid for the synthetic magnetic intensity but has little effect on the component fluctuation caused by the misalignment error. Compared with the traditional method, the proposed calibration method is not only effective for the synthetic magnetic intensity, but also has a good suppression effect on the component fluctuation.

The above experimental results show that the proposed method can calibrate the errors of the magnetometer and misalignment in the magnetic vector measurement system simultaneously and accurately.

6. Discussion

(1) The use of the plane compression method in ellipsoid fitting enables misalignment errors to be calibrated simultaneously with magnetometer errors. This simplifies the calibration process of the magnetic vector measurement system and makes it convenient for use. In addition, the method has the potential to be applied to other vector measurement systems.

(2) The proposed method does not require a magnetic field generator and planar positioning device. It eliminates the need for additional mechanical devices to construct constraints for solving error parameters. This avoids the introduction of additional error sources and has the benefit of higher accuracy and stability of the proposed method.

(3) The proposed method has requirements for the coverage of the data to the space. When the data can comprehensively cover the spatial angle, the calibration accuracy will reach its best result. How to increase the data coverage of the space via an algorithm is one of our future research directions.

(4) The optimum accuracy of the proposed method is limited by the angular measurement accuracy of the INS. The pairwise vector subtraction method in equation (20) can reduce the influence of INS random errors on the solution of systematic error parameters. However, random errors in attitude data will still cause component fluctuations when restoring magnetic vector data to geographic coordinates.

7. Conclusion

This paper proposed a new method for the calibration of a magnetic vector measurement system. The method innovatively applies the theory of plane compression. It removes the dependence of calibration constraints on the rotation of the planar positioning device or machining device with a special angle. Therefore, the calibration can be quickly performed via simple operations and few experiments. The theoretical feasibility of the method is verified by the simulation experiment. The accuracy and robustness of the method in application are verified by four replicate experiments in the same location.

The experiment results indicate that the method can contribute to the accuracy improvement of magnetic vector measurement systems.

Data availability statement

All data that support the findings of this study are included within the article (and any supplementary files).

Acknowledgments

ORCID iDs

Supeng Li https://orcid.org/0000-0002-8926-7654
Jing Zhao https://orcid.org/0000-0002-3382-9187

References

[1] Barczyk M and Lynch A F 2012 Integration of a triaxial magnetometer into a helicopter UAV GPS-aided INS *IEEE Trans. Aerosp. Electron. Syst.* **48** 2947–60

[2] No H and Kee C 2019 Enhancement of GPS/INS navigation system observability using a triaxial magnetometer *Trans. Japan Soc. Aeronaut. Space Sci.* **62** 125–36

[3] Ghasemi-Moghadam S and Homaeinezhad M R 2018 Attitude determination by combining arrays of MEMS accelerometers, gyros, and magnetometers via quaternion-based complementary filter *Int. J. Numer. Modelling, Electron. Netw. Devices Fields* **31** e2282

[4] Kim K-Y, Jeong E, Kim S and Shin Y 2019 Magnetic anomaly detection using continuous angle alignment of three-axis magnetic signal *IEEE Sens. J.* **19** 743–50

[5] Chilo J, Jabor A, Lizska L, Eide Å J and Lindblad T 2007 Obtaining "images" from iron objects using a 3-axis fluxgate magnetometer *Nucl. Instrum. Methods Phys. Res. A* **580** 1105–9

[6] Liu S, Hu X and Zhu R 2018 Joint inversion of surface and borehole magnetic data to prospect concealed orebodies: a case study from the Mengku iron deposit, northwestern China *J. Appl. Geophys.* **154** 150–8

[7] Liu S, Hu X, Zhang H, Geng M and Zuo B 2017 3D magnetization vector inversion of magnetic data: improving and comparing methods *Pure Appl. Geophys.* **174** 4421–44

[8] Zikmund A, Janosek M, Ulvr M and Kupec J 2015 Precise calibration method for triaxial magnetometers not requiring Earth's field compensation *IEEE Trans. Instrum. Meas.* **64** 1242–7

[9] Pan D, Li J, Jin C, Liu T, Lin S and Li L 2020 A new calibration method for triaxial fluxgate magnetometer based on magnetic shielding room *IEEE Trans. Ind. Electron.* **67** 4183–92

[10] Merayo J M G, Brauer P, Primdahl F, Petersen J R and Nielsen O V 2000 Scalar calibration of vector magnetometers *Meas. Sci. Technol.* **11** 120–32

[11] Alonso R and Shuster M D 2002 TWOSTEP: a fast robust algorithm for attitude-independent magnetometer-bias determination *J. Astronaut. Sci.* **50** 433–4

[12] Alonso R and Shuster M D 2002 Complete linear attitude-independent magnetometer calibration *J. Astronaut. Sci.* **50** 477–4

[13] Xiaoming Z, Guobin C, Jie L and Jun L 2014 Calibration of triaxial MEMS vector field measurement system *IET Sci. Meas. Technol.* **8** 601–9

[14] Crassidis J L, Lai K-L and Harman R R 2005 Real-time attitude-independent three-axis magnetometer calibration *J. Guid. Control Dyn.* **28** 115–20

[15] Yu H, Ye L, Guo Y and Su S 2021 An effective in-field calibration method for triaxial magnetometers based on local magnetic inclination *IEEE Trans. Instrum. Meas.* **70** 1–9

[16] Li X and Li Z 2012 A new calibration method for tri-axial field sensors in strap-down navigation systems *Meas. Sci. Technol.* **23** 105105

[17] Li X, Song B, Wang Y, Niu J and Li Z 2018 Calibration and alignment of tri-axial magnetometers for attitude determination *IEEE Sens. J.* **18** 7399–406

[18] Pang H, Zhu X, Pan M, Zhang Q, Wan C, Luo S, Chen D, Chen J, Li J and Lv Y 2016 Misalignment calibration of geomagnetic vector measurement system using parallelepiped frame rotation method *J. Magn. Magn. Mater.* **419** 309–16

[19] Wan C, Pan M, Zhang Q, Pang H, Zhu X, Pan L, Sun X and Wu F 2017 Improved component compensation for geomagnetic field vector measurement using Lagrange multiplier method *IET Sci. Meas. Technol.* **11** 1094–8

[20] Gao Q, Cheng D, Wang Y, Li S and Zhao J 2019 A calibration method for the misalignment error between inertial navigation system and tri-axial magnetometer in three-component magnetic measurement system *IEEE Sens. J.* **19** 12217–23

[21] Baritzhack I Y 1989 Extension of Euler's theorem to n-dimensional spaces *IEEE Trans. Aerosp. Electron. Syst.* **25** 903909

[22] Panou G and Agatza-Balodimou A-M 2021 Direct and indirect estimation of the variance–covariance matrix of the parameters of a fitted ellipse and a triaxial ellipsoid *J. Surv. Eng.* **147** 04020026

[23] Wang D W 2003 Analysis of the international geomagnetic reference field error in the China continent *Chin. J. Geophys. Chin. Ed.* **46** 171–4